PAPER

Broadband infrared circular dichroism in chiral metasurface absorbers

View the article online for updates and enhancements.

IOP ebooks™

Bringing together innovative digital publishing with leading authors from the global scientific community.

Start exploring the collection–download the first chapter of every title for free.

Broadband infrared circular dichroism in chiral metasurface absorbers

Leixin Ouyang[1]**, Daniel Rosenmann**[2]**, David A Czaplewski**[2]**, Jie Gao**[1]
and Xiaodong Yang[1] (ORCID)

[1] Department of Mechanical and Aerospace Engineering, Missouri University of Science and Technology, Rolla, MO 65409, United States of America
[2] Center for Nanoscale Materials, Argonne National Laboratory, Argonne, IL 60439, United States of America

E-mail: gaojie@mst.edu and yangxia@mst.edu

Abstract

Chirality is ubiquitous in nature and it is essential in many fields, but natural materials possess weak and narrow-band chiroptical effects. Here, chiral plasmonic metasurface absorbers are designed and demonstrated to achieve large broadband infrared circular dichroism (CD). The broadband chiral absorber is made of multiple double-rectangle resonators with different sizes, showing strong absorption of left-handed or right-handed circularly polarized (LCP or RCP) light above 0.7 and large CD in absorption more than 0.5 covering the wavelength range from 1.35 μm to 1.85 μm. High broadband polarization-dependent local temperature increase is also obtained. The switchable infrared reflective chiral images are further presented by changing the wavelength and polarization of incident light. The broadband chiral metasurface absorbers promise future applications in many areas such as polarization detection, thermophotovoltaics, and chiral imaging.

Keywords: Chiral metasurface, circular dichroism, broadband, chiral image

(Some figures may appear in colour only in the online journal)

1. Introduction

Chirality plays an important role in many fields, ranging from chemistry, biology, to physics, and the study of chirality has led to many discoveries in science and technology [1, 2]. Optical chiral materials usually have two enantiomeric forms, which exhibit different optical responses to the incident LCP and RCP light [3]. Natural materials generally possess very weak and narrow-band chiroptical effects. One solution is to use the recently developed metamaterials and metasurfaces [4–8] to enhance the chiroptical effects with different kinds of optical structures, such as pyramids [9], double-layer ellipses [10], twisted E-shaped resonators [11], double-bar patterns [12], Gamma-like array [13], gammadion patterns [14], L-shaped patterns [15, 16], nanoaperture antennas [17, 18], and liquid-crystal-loaded resonators [19]. Recently, it has been demonstrated that the CD in a chiral plasmonic metasurface occurs due to the polarization-dependent optical energy distribution and Ohmic heat dissipation [20]. Most of the broadband

achiral plasmonic metasurface absorbers have been designed by simply combining multiple plasmonic resonators with different sizes altogether into one unit cell, where achiral plasmonic resonators with various geometries such as patch, cross, disk and ring have been adopted [21–25]. Broadband absorption is then achieved through regulating the coupled multiple plasmonic resonances with predefined distances within the desired wavelength range. Such design method can also be applied to create broadband chiral metasurface absorbers. One important application for chiral metamaterials and metasurfaces is chiral imaging for achieving distinct displayed images by switching the incident circular polarization [26–32]. By encoding the image with chiral nanostructures as image pixels, different image patterns can be visualized for LCP and RCP light by locally switching on or off the pixels.

Here, broadband chiral plasmonic metasurface absorbers are designed and demonstrated to achieve strong absorption of LCP or RCP light above 0.7 and large infrared CD more than 0.5 covering the wavelength range from 1.35 μm to 1.85 μm.

The designed chiral absorber is based on a three-layer metal-dielectric-metal structure. The broadband chiral absorbers are developed by combining multiple double-rectangle resonators into one unit cell in infrared regime. In order to understand the mechanism of the broadband optical absorption of LCP or RCP light, the electric field distributions and temperature distributions under circular polarizations are simulated. As one potential application for the demonstrated broadband chiral metasurface absorbers, the high-contrast switchable infrared reflective chiral images of a pie-like pattern are further presented, by varying the incident wavelength and polarization. The results in chiral imaging promise future applications in data encryption [33], dynamic display [34], chemical analysis and biosensing [35] and information processing [36]. Our results also show many other applications such as polarization detection [37], thermophotovoltaics [11, 15] and optical holography [38].

2. Design and characterization of broadband chiral absorbers

The chiral metasurface absorber is designed with a three-layer metal-dielectric-metal structure including the double rectangle resonators in the top gold (Au) layer with the thickness of 55 nm, the silica (SiO$_2$) dielectric layer with the thickness of 130 nm, and the gold mirror layer with the thickness of 200 nm deposited on glass substrate. Figures 1(a) and (b) show the schematics of the unit cells in two enantiomeric forms of Form A and Form B for the broadband chiral metasurface absorber, by combining six individual double-rectangle resonators with different sizes. The double-rectangle pattern contains two position-shifted rectangles for breaking mirror symmetries, and the chiral resonant absorption is further enhanced inside the three-layer structure working as the chiral Fabry-Pérot cavity [13]. Each double-rectangle resonator exhibits narrow-band chiroptical response around a certain wavelength so that the six resonators in total in one unit cell will achieve broadband chiroptical performance. The double-rectangle pattern is made of two connected identical gold rectangles with length L, width W, and overlapped space OP, and the resonators within one unit cell are marked from 1 to 5 in figure 1(c). The vertical and horizontal periods of the unit cell are P_x and P_y, respectively. The designed geometric parameters *are $L_1 \sim L_5$ =* 300, 410, 475, 540, 610 nm, W = 135 nm, OP = 10 nm, P_x = 1140 nm and P_y = 2110 nm. It is noted that two identical double-rectangle resonators with L_3 in the unit cell are adopted to get the optimized CD around the wavelength of 1.55 μm due to the coupling between neighboring resonators, according to the numerical simulation. Due to the thick gold mirror layer, the transmission is negligible ($T = 0$) and the absorption can be calculated as $A = 1-R$, where A, T and R denote the absorption, transmission and reflection, respectively). Since the two enantiomer forms of Form A and Form B shown in figures 1(a) and (b) have opposite chiroptical response under circular polarization, only the absorption performance of the chiral absorber in Form A is analyzed. The three-layer structure is deposited on a glass
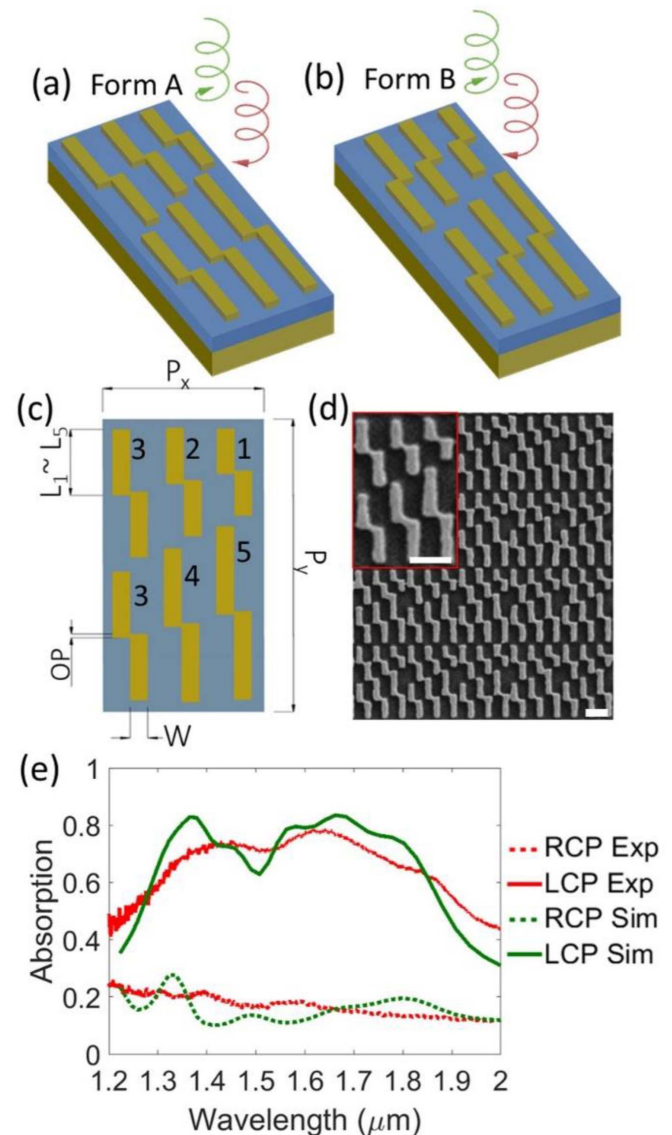
Figure 1. (a), (b) Schematics of the unit cells in two enantiomeric forms of Form A and Form B for the broadband chiral metasurface absorber. (c) Top-view schematics of Form A with the designed geometric parameters. (d) SEM image of the fabricated broadband chiral absorber in Form A. Scale bar represents 500 nm. (e) Measured and simulated absorption spectra of the broadband chiral metasurface absorber in Form A under LCP and RCP incidence.

substrate, where the Au layers are deposited using a Lesker PVD250 electron beam evaporator and the SiO$_2$ dielectric layer is deposited by reactive sputtering (Lesker CMS18 system). Next, the designed chiral metasurface absorbers are fabricated by using focused ion beam (FIB) milling (FEI Helios Nanolab 600) to mill the top gold layer into the desired double-rectangle patterns. Figure 1(d) shows the scanning electron microscope (SEM) image of the top view of the fabricated broadband chiral absorber in Form A. The Fourier transform infrared spectrometer (FTIR, Nicolet 6700) and a connected infrared microscope are used to measure the optical reflection spectra through a 15x reflective Cassegrain objective, with the incident circular polarization specified by a set of linear polarizer and quarter-wave plate. The absorption of LCP and
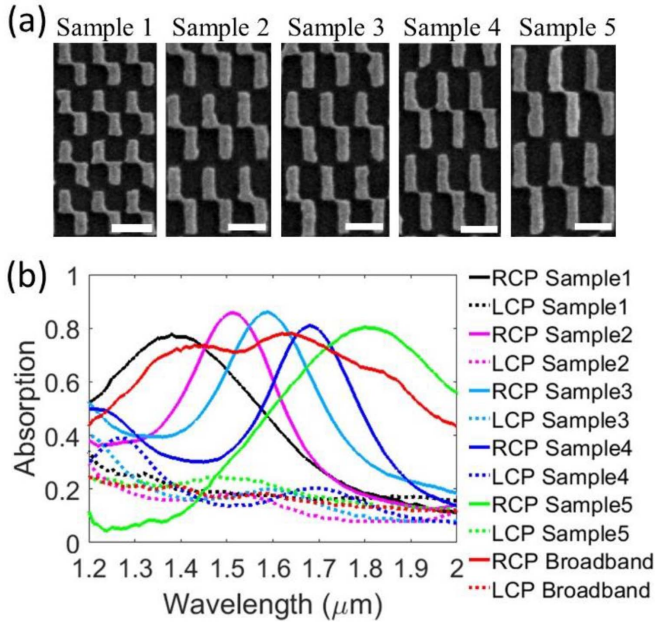
Figure 2. (a) SEM images of the fabricated narrow-band chiral absorbers in Form A from Sample 1 to Sample 5. Scale bar represents 500 nm. (b) Measured corresponding absorption spectra for each sample under LCP and RCP incidence.

Figure 3. (a) Simulated electric field distributions in the plane 5 nm below the gold rectangle patterns under LCP and RCP incidence at different resonance wavelength. (b) Simulated distributions of the difference of local temperature increase between LCP and RCP incidence at the top surface of the double-rectangle patterns.

RCP light is also simulated by using the finite element method solver (COMSOL Multiphysics, RF Module), where periodic boundary conditions are employed along both *x* and *y* directions in the unit cell. For simulating the optical properties, only a 200 nm-thick glass substrate is used since the thick gold mirror layer blocks almost all the transmitted light. The permittivity of gold is taken from the standard experimental data of Johnson and Christy [39] with the imaginary part increased by a factor of 3. Due to the gallium ion contamination during the FIB process, surface scattering and grain boundary effects in the fabricated thin gold layer [40, 41], the imaginary part of the permittivity of gold is increased in the simulations in order to match the experimental results. The refractive index of glass is set to a constant value of 1.45. Figure 1(e) presents the measured and simulated absorption spectra of the broadband chiral metasurface absorber in Form A under LCP and RCP incidence. The observed absorption is above 0.7 under RCP incidence, and the measured CD in absorption ($CDA = |A_{LCP} - A_{RCP}|$) is more than 0.5 in the wavelength range from 1.35 μm through 1.85 μm. Some difference between the simulated and measured absorption spectra is possibly caused by the sample defects such as the varying gap sizes between the neighboring resonators and the side wall roughness from the FIB milling process, as well as the oblique incident angle through the reflective Cassegrain objective.

For comparison, the narrow-band chiral metasurface absorbers of each kind with only a single double-rectangle resonator present in one unit cell are fabricated and characterized, with $P_x = 380$ nm and $P_y = 700$, 870, 1000, 1130 and 1260 nm from Sample 1 to Sample 5, respectively. Figure 2(a) shows the top-view SEM images of the fabricated narrow-band chiral absorbers in Form A for the five samples. The
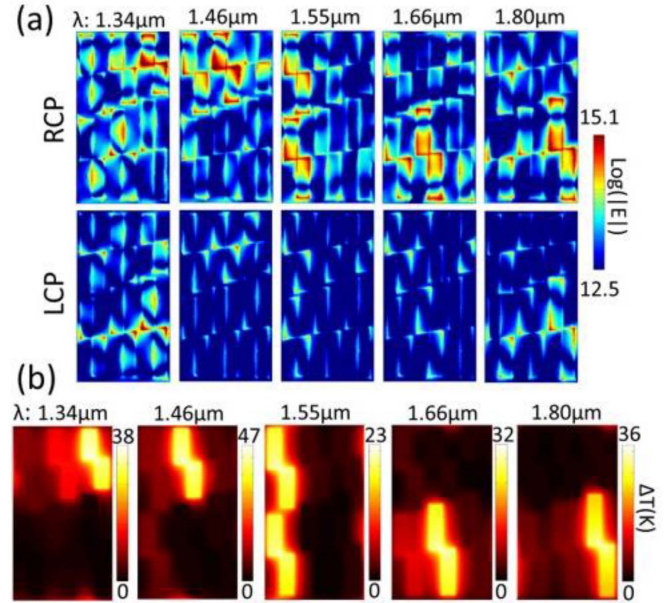
measured corresponding absorption spectra plotted in figure 2(b) shows that each kind of double-rectangle resonator exhibits a high CDA up to 0.6 and occupies a limited absorption band from short wavelength to long wavelength as the rectangle length increases. Once all the resonators are combined to form the broadband absorber, the CDA slightly drops due to the coupling effects between the adjacent resonators, showing the tradeoff between the broad bandwidth and the high CDA.

In order to understand the mechanism of the broadband absorption of circularly polarized light, the electric field distributions and temperature distributions in the chiral metasurface absorbers in Form A are simulated. The electric field distributions in the plane 5 nm below the gold rectangle patterns are shown in figure 3(a) under circular polarizations at different wavelengths. It shows that multiple chiral plasmonic resonances are enhanced within the dielectric layer under RCP incidence, but are significantly suppressed under LCP incidence. Each double-rectangle resonator is excited at a different resonance wavelength, so that overall the combined multiple resonators give strong broadband chiroptical response. It also shows the coupling between the neighboring resonators, which will cause the resonance peak shifts. The absorbed light energy will be transferred into heat, where the heat generation density in metal can be calculated as $q(r) = (\omega/2)Im[\varepsilon(\omega)]\varepsilon_0|E(r)|^2$. The heat transfer equation $\nabla \cdot (-k\nabla T) = q$ can be solved by using the finite element method solver (COMSOL Multiphysics, Heat Transfer Module) to get the temperature distribution in the absorber, where T is the temperature and k is the thermal conductivity of the material. For simulating the heat transfer problem, a 100 μm-thick glass substrate is considered below the thick gold mirror layer. The boundary conditions are specified as the fixed temperature of 273 K at the top surface of
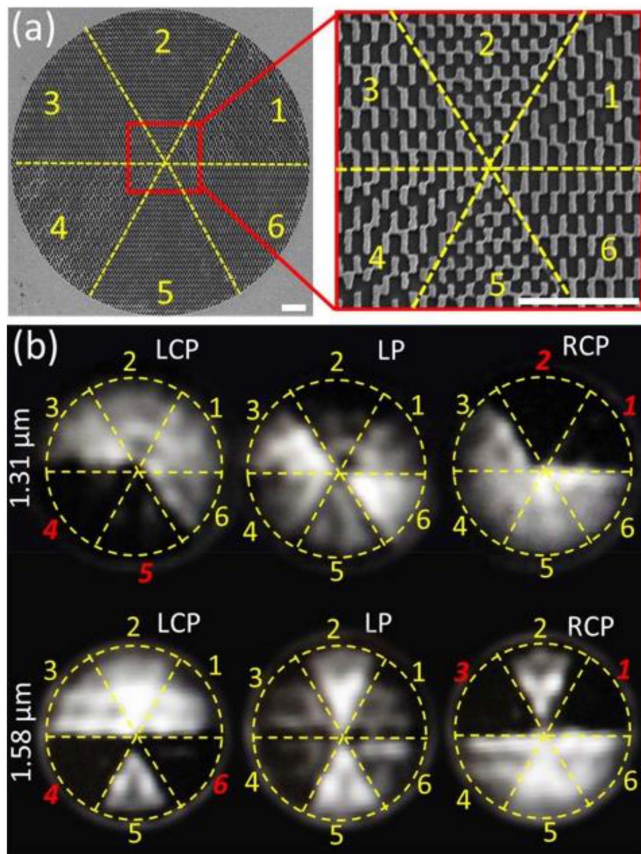
Figure 4. (a) SEM images of the pie-like pattern with six cells made of different types of chiral absorbers. Scale bar represents 3 μm. (b) The chiral reflective images of the six cells at the wavelengths of 1.31 and 1.58 μm under LCP and RCP incidence.

the air and the bottom surface of the glass substrate, and the thermal insulation at the periodic side surfaces. The heat is mainly generated inside the top gold patterns, since the dielectric spacer layer and air have relatively low thermal conductivity. Once the whole system reaches thermal equilibrium, the top gold patterns have much higher temperatures compared to the surrounding materials. The incident optical power is fixed at 50 μW per unit cell. Figure 3(b) presents the difference of the local temperature increase for the chiral absorber under LCP and RCP incidence ($\Delta T = |T_{LCP}-T_{RCP}|$) at the top surface of the double-rectangle patterns, which can go up to 47 K. It shows that as the incident wavelength increases, the high temperature locations shift from small resonator to large resonator. The high broadband polarization-dependent local temperature increase is caused by the corresponding strong broadband CDA.

3. Near-infrared reflective chiral images

Next, the high-contrast switchable infrared reflective chiral images of a pie-like pattern are presented, by varying the incident wavelength and polarization. Figure 4(a) shows the SEM image of the pie-like pattern with a diameter of 45 μm, which includes six cells with different types of chiral absorbers. The zoom-in SEM image of the central part is also shown. Cell

1 and Cell 4 have the broadband chiral absorbers in Form A and Form B that can work from 1.35 to 1.85 μm, respectively. Cell 2 and Cell 5 include the narrow-band chiral absorbers at the resonance of 1.3 μm in Form A and Form B, respectively. Cell 3 and Cell 6 have the narrow-band chiral absorbers at the resonance of 1.55 μm in Form A and Form B, respectively. Then the pie-like pattern is illuminated by the normally incident laser beam at two wavelengths of 1.31 and 1.58 μm from fiber-coupled laser diodes under two circular polarizations through a 20x microscope objective lens, where the incident circular polarization is specified using a set of linear polarizer and quarter-wave plate placed before the objective lens. The reflected light from the pie-like pattern is separated by a beam splitter and then captured by a near-infrared camera. Figure 4(b) shows the reflective images of the six cells under LCP, RCP and linear polarization (LP) incidence at two different wavelengths. Due to the different working wavelengths and the two forms of chiral absorbers, the reflective images show distinct bright and dark areas. Here the brightness of each cell is proportional to its reflection, so that high brightness represents low absorption and thus low temperature in the cell. For the incident LCP (or RCP) light at the wavelength of 1.31 μm, Cell 4 and Cell 5 (or Cell 1 and Cell 2) are much darker than the surrounding areas. But for the incident LCP (or RCP) light at 1.58 μm, instead, Cell 4 and Cell 6 (or Cell 1 and Cell 3) are dark. Under the incident LP light at any of the two wavelengths, all six cells are bright although the brightness is different. It shows that the chiral reflective images from the sample can be switched according to the different combinations of incident wavelength and polarization.

4. Conclusion

In summary, chiral plasmonic metasurface absorbers are designed and demonstrated to achieve large broadband infrared circular dichroism in absorption as well as high broadband polarization-dependent local temperature increase. The broadband chiral metasurface absorbers are made of multiple narrow-band chiral resonators with different sizes. The switchable infrared reflective chiral images controlled by the incident wavelength and polarization are also demonstrated. These results present future promising applications in polarization detection, thermal energy harvesting, molecular sensing, and chiral imaging.

from the Intelligent Systems Center and the facility support from the Materials Research Center at Missouri S&T.

ORCID iD

Xiaodong Yang ⓘ https://orcid.org/0000-0001-9031-3155

References

[1] Greenfield N J 2007 Using circular dichroism spectra to estimate protein secondary structure *Nat. Protoc.* **1** 2876

[2] Li X, Yu L, Yu L, Dong Y, Gao Q, Yang Q, Yang W, Zhu Y and Fu Y 2018 Chiral polyaniline with superhelical structures for enhancement in microwave absorption *Chem. Eng. J.* **352** 745–55

[3] Plum E and Zheludev N I 2015 Chiral mirrors *Appl. Phys. Lett.* **106** 221901

[4] Pendry J B 2000 Negative refraction makes a perfect lens *Phys. Rev. Lett.* **85** 3966–9

[5] Smith D R, Pendry J B and Wiltshire M C K 2004 Metamaterials and negative refractive index *Science* **305** 788–92

[6] Yao K and Liu Y 2014 Plasmonic metamaterials *Nanotechnol. Rev.* **3** 177–210

[7] Collins J T, Kuppe C, Hooper D C, Sibilia C, Centini M and Valev V K 2017 Chirality and chiroptical effects in metal nanostructures: fundamentals and current trends *Adv. Opt. Mater.* **5** 1700182

[8] Luo Y, Chi C, Jiang M, Li R, Zu S, Li Y and Fang Z 2017 Plasmonic chiral nanostructures: chiroptical effects and applications *Adv. Opt. Mater.* **5** 1700040

[9] McPeak K M, Engers C D V, Blome M, Park J H, Burger S, Gosálvez M A, Faridi A, Ries Y R, Sahu A and Norris D J 2014 Complex chiral colloids and surfaces via high-index off-cut silicon *Nano Lett.* **14** 2934–40

[10] Rodrigues S P, Lan S, Kang L, Cui Y, Panuski P W, Wang S, Urbas A M and Cai W 2017 Intensity-dependent modulation of optically active signals in a chiral metamaterial *Nat. Commun.* **8** 14602

[11] Lv T T, Li Y X, Ma H F, Zhu Z, Li Z P, Guan C Y, Shi J H, Zhang H and Cui T J 2016 Hybrid metamaterial switching for manipulating chirality based on VO2 phase transition *Sci. Rep.* **6** 23186

[12] Ouyang L, Wang W, Rosenmann D, Czaplewski D A, Gao J and Yang X 2018 Near-infrared chiral plasmonic metasurface absorbers *Opt. Express.* **26** 31484–9

[13] Tang B, Li Z, Palacios E, Liu Z, Butun S and Aydin K 2017 Chiral-selective plasmonic metasurface absorbers operating at visible frequencies *IEEE Photonics Technol. Lett.* **29** 295–8

[14] Zhu A Y, Chen W T, Zaidi A, Huang Y W, Khorasaninejad M, Sanjeev V, Qiu C W and Capasso F 2018 Giant intrinsic chiro-optical activity in planar dielectric nanostructures *Light Sci. Appl.* **7** 17158

[15] Kong X T, Khorashad L K, Wang Z and Govorov A O 2018 Photothermal circular dichroism induced by plasmon resonances in chiral metamaterial absorbers and bolometers *Nano Lett.* **18** 2001–8

[16] Yin S, Xiao D, Liu J, Li K, He H, Jiang S, Luo D, Sun X, Ji W and Liu Y 2018 Reconfigurable chiral metasurface absorbers based on liquid crystals *IEEE Photonics J.* **10** 4600909

[17] Jia Y P, Zhang Y L, Dong X Z, Zheng M L, Li J, Liu J, Zhao Z S and Duan X M 2014 Complementary chiral metasurface with strong broadband optical activity and enhanced transmission *Appl. Phys. Lett.* **104** 011108

[18] Wang Z, Teh B, Wang Y, Adamo G, Teng J and Sun H 2017 Enhancing circular dichroism by super chiral hot spots from a chiral metasurface with apexes *Appl. Phys. Lett.* **110** 221108

[19] Xiao D, Liu Y J, Yin S, Liu J, Ji W, Wang B, Luo D, Li G and Sun X W 2018 Liquid-crystal-loaded chiral metasurfaces for reconfigurable multiband spin-selective light absorption *Opt. Express.* **26** 25305–14

[20] Khanikaev A B *et al* 2016 Experimental demonstration of the microscopic origin of circular dichroism in two-dimensional metamaterials *Nat. Commun.* **7** 12045

[21] Lefebvre A, Costantini D, Doyen I, Lévesque Q, Lorent E, Jacolin D, Greffet J J, Boutami S and Benisty H 2016 CMOS compatible metal-insulator-metal plasmonic perfect absorbers *Opt. Mater. Express* **6** 2389–96

[22] Liu X, Tyler T, Starr T, Starr A F, Jokerst N M and Padilla W J 2011 Taming the blackbody with infrared metamaterials as selective thermal emitters *Phys. Rev. Lett.* **107** 045901

[23] Cheng C W, Abbas M N, Chiu C W, Lai K T, Shih M H and Chang Y C 2012 Wide-angle polarization independent infrared broadband absorbers based on metallic multi-sized disk arrays *Opt. Express.* **20** 10376–81

[24] Deng H, Stan L, Czaplewski D A, Gao J and Yang X 2017 Broadband infrared absorbers with stacked double chromium ring resonators *Opt. Express.* **25** 28295–304

[25] Li Z, Stan L, Czaplewski D A, Yang X and Gao J 2018 Wavelength-selective mid-infrared metamaterial absorbers with multiple tungsten cross resonators *Opt. Express.* **26** 5616–31

[26] Rodrigues S P, Lan S, Kang L, Cui Y and Cai W 2014 Nonlinear imaging and spectroscopy of chiral metamaterials *Adv. Mater.* **26** 6157–62

[27] Khorasaninejad M, Chen W T, Zhu A Y, Oh J, Devlin R C, Rousso D and Capasso F 2016 Multispectral chiral imaging with a metalens *Nano Lett.* **16** 4595–600

[28] Kang L, Rodrigues S P, Taghinejad M, Lan S, Lee K T, Liu Y, Werner D H, Urbas A and Cai W 2017 Preserving spin states upon reflection: linear and nonlinear responses of a chiral meta-mirror *Nano Lett.* **17** 7102–9

[29] Wang Q, Plum E, Yang Q, Zhang X, Xu Q, Xu Y, Han J and Zhang W 2018 Reflective chiral meta-holography: multiplexing holograms for circularly polarized waves *Light Sci. Appl.* **7** 25

[30] Chen Y, Gao J and Yang X 2018 Direction-controlled bifunctional metasurface polarizers *Laser Photonics Rev.* **12** 1800198

[31] Chen Y, Gao J and Yang X 2018 Chiral metamaterials of plasmonic slanted nanoapertures with symmetry breaking *Nano Lett.* **18** 520–7

[32] Chen Y, Gao J and Yang X 2019 Chiral grayscale imaging with plasmonic metasurfaces of stepped nanoapertures *Adv. Opt. Mater.* **7** 1801467

[33] Chen Y, Yang X and Gao J 2019 3D Janus plasmonic helical nanoapertures for polarization-encrypted data storage *Light Sci. Appl.* **8** 45

[34] Chen Y, Duan X, Matuschek M, Zhou Y, Neubrech F, Duan H and Liu N 2017 Dynamic color displays using stepwise cavity resonators *Nano Lett.* **17** 5555–60

[35] Chen X, Huang Z, Chen S Y, Li K, Yu X Q and Pu L 2010 Enantioselective gel collapsing: a new means of visual chiral sensing *J. Am. Chem. Soc.* **132** 7297–9

[36] Silva A, Monticone F, Castaldi G, Galdi V, Alù A and Engheta N 2014 Performing mathematical operations with metamaterials *Science* **343** 160–3

[37] Li W, Coppens Z J, Besteiro L V, Wang W, Govorov A O and Valentine J 2015 Circularly polarized light detection with

hot electrons in chiral plasmonic metamaterials *Nat. Commun.* **6** 8379

[38] Chen Y, Yang X and Gao J 2018 Spin-controlled wavefront shaping with plasmonic chiral geometric metasurfaces *Light Sci. Appl.* **7** 84

[39] Johnson P B and Christy R W 1972 Optical constants of the noble metals *Phys. Rev.* B **6** 4370–9

[40] Liu N, Langguth L, Weiss T, Kästel J, Fleischhauer M, Pfau T and Giessen H 2009 Plasmonic analogue of electromagnetically induced transparency at the Drude damping limit *Nat. Mater.* **8** 758–62

[41] Wan W, Yang X and Gao J 2016 Strong coupling between mid-infrared localized plasmons and phonons *Opt. Exp.* **24** 12367–74